

# Transverse Momentum Structure of Diffractive DIS Models

J.C. Williams\*

Theoretical Physics, Oxford University,  
1 Keble Road,  
Oxford, OX1 3NP, U.K.

September 7, 2018

## Abstract

The transverse momentum distribution of the diffractive final state provides an interesting test of models of diffractive deep-inelastic scattering at HERA. We present a comparison of several colour-singlet exchange models with thrust transverse momentum data from a recent H1 analysis. We also study the effect of constraints imposed on the kinematically-accessible phase space by data selection cuts and find that, as a result of the pseudo-rapidity cut which is used by H1 to select diffractive events, there is no dijet contribution at low transverse momenta. We are able to fit the large transverse momentum part of the data with a two-gluon dijet model. The results of this analysis are compared with a previous study of large pseudo-rapidity gap structure function data, and we discuss ways in which one might reconcile the results of the two analyses. We conclude that a significant small- $\beta$  3-jet contribution is probably required to explain the data, and show that the combination of a two-gluon dijet model and an exponentially-decaying thrust transverse momentum distribution provides a good fit over the entire kinematic range of the thrust data.

## 1 Introduction

With the increasing numbers of models [1–8] which propose to describe diffractive deep-inelastic scattering (DIS), it is important to find ways to test them. One method is to examine events with a large pseudo-rapidity gap between the proton remnant and the diffractive final state. The requirement of a large pseudo-rapidity gap means that the experimental cuts are selecting a sample with a strongly reduced phase space [1]. An analysis of the effects of pseudo-rapidity cuts in terms of diffractive structure functions has been reported previously [9]. A further test of models of diffractive DIS is to study the unintegrated transverse momentum distribution of diffractive events [10–12].

---

\*email: j.williams1@physics.ox.ac.uk

Here we provide a detailed analysis of the thrust transverse momentum distribution reported recently by H1 [13]. We study the restrictions on available phase space for diffractive interactions which are imposed by a combination of pseudo-rapidity cuts and other data selection cuts. We find that these cuts reject dijet (quark–antiquark diffractive final state) events with small transverse momenta relative to the virtual photon–proton axis. An additional contribution is therefore required to fit the data at small transverse momenta. At the values at which the low-momentum dijet cut-off occurs the data also changes slope, having an approximately quadratic fall-off with increasing transverse momentum up to about  $4\text{--}10\text{ GeV}^2$  which changes to a quartic fall-off at larger transverse momenta. The ( $\beta$ -dependent) position of the low transverse momentum dijet cut-off corresponds rather closely to the transverse momentum values at which the slope of the cross section changes.

In this paper we consider how dijet events contribute to the transverse momentum distribution, and discuss the rôle that higher-multiplicity diffractive final-state events are expected to play. The colour-singlet exchange models of dijet production which we consider here are: the form factor vector pomeron models of Donnachie and Landshoff (D-L) [2, 3] and Ellis and Ross (E-R) [1, 9] (in the Feynman gauge and in a non-covariant gauge), the scalar pomeron model of Vermaseren *et al* [4], a leading-twist single-gluon exchange model, and the two-gluon Landshoff-Nachtmann model described in [6]. The Donnachie-Landshoff (non-covariant gauge) and two-gluon models provide a good fit to the quartic fall-off of the diffractive cross section with thrust transverse momentum, while the other models predict only a quadratic fall at large transverse momenta.

The result of the thrust transverse momentum analysis appears, at first, rather in contradiction with a recent analysis of large pseudo-rapidity gap structure function data [9]. The structure function analysis appeared to strongly favour the  $1/p_\perp^2$  models. In particular, the E-R and leading-twist models fit the structure function data well over a wide range of  $Q^2$ ,  $\beta$  and  $x_P$ . The two-gluon and Donnachie-Landshoff models fall off too rapidly with decreasing  $\beta$  to fit the data without a substantial contribution from higher-order diffractive final states. We explore two possible ways to reconcile these results: the first is to consider that the models which give a quadratic dijet transverse momentum dependence describe the diffractive data only at large  $\beta$ , while the small- $\beta$  spectrum is dominated by a two-gluon-like contribution. This is a possibility that cannot be ruled out by present large pseudo-rapidity gap data. The other explanation for these results is that both sets of data might be described by the combination of a two-gluon dijet component and a (possibly non-perturbative) contribution which is strongly peaked at small  $\beta$  and small thrust transverse momentum.

The position of the low transverse momentum cut-off is largest at small values of  $\beta$ . This means that the extra thrust transverse momentum contribution which is required to “fill in” the thrust transverse momentum distribution spectrum is greatest at large diffractive masses, i.e., at small  $\beta$ . Since  $\beta$  plays the rôle of the scaling variable  $x$  in standard DIS, we conclude that the additional contribution is probably due to the gluonic structure of the pomeron. That is, the additional contribution needed to describe the thrust transverse momentum spectrum at small transverse momenta is probably due to 3-or-more parton diffractive final states, predominantly quark–antiquark–gluon (“3-jet”) diffractive final states. Another reason for this conclusion is that most of the H1 thrust transverse momentum distribution data corresponds to very small values of  $\beta$ , and it is at such values that one might expect the contribution from 3-jet final states to be significant [8, 14, 15]. The combination of a two-gluon dijet model and a simple  $\beta$ -dependent Gaussian fits the data well over the entire kinematic range in the H1 analysis.

The rest of this paper is organized as follows: in Sect. 2 we present a discussion of the usual diffractive DIS kinematics, in which we introduce the kinematic variables which are of particular interest in this analysis. Sect. 3 contains an analysis of the effects of data selection cuts. In Sect. 4 we describe several models of diffractive dijet production and compare these models with thrust transverse momentum data from a recent H1 study [13]. In Sect. 5 we compare our results with a recent analysis of large pseudo-rapidity gap structure function data and discuss two possible ways to reconcile the two analyses. This section includes a discussion of the possible contribution of 3-jet diffractive final states to the transverse momentum spectrum. Sect. 6 summarises the results presented in this paper and outlines further investigations which could be carried out to verify our conclusions. In the Appendix we give a brief discussion of the large pseudo-rapidity gap structure function analysis carried out previously [9]. In this Appendix we extend the comparison of form factor models with large pseudo-rapidity gap structure function data to allow for a different form factor cut-off,  $\Lambda$ , and include fits for the form factor models calculated in the non-covariant gauge.

## 2 Background

### 2.1 Kinematics

#### 2.1.1 Standard Kinematics

In the HERA electron–proton experiments 820 GeV protons<sup>1</sup> collide with 27.5 GeV electrons or positrons. This corresponds to a centre-of-mass (CMS) energy of  $\sqrt{S_{\text{Tot}}} \sim 300$  GeV. In the HERA lab frame the positive  $z$ -axis is defined by the forward proton direction with the origin at the interaction vertex. We consider diffractive deep-inelastic  $e - P$  scattering,

$$e(p_e) + P(P) \rightarrow e(p'_e) + P(P') + X(X), \quad (1)$$

where the momenta of the particles are shown in brackets. One may consider that the interaction proceeds by virtual photon–pomeron deep-inelastic scattering,

$$\gamma^*(q) + \mathbb{P}(P_{\mathbb{P}}) \rightarrow X(X), \quad (2)$$

where  $P_{\mathbb{P}} = P - P'$ .

We use the usual kinematic variables of deep-inelastic scattering,

$$Q^2 = -q^2, \quad x = \frac{Q^2}{2P \cdot q}, \quad \text{and} \quad y = \frac{Q^2}{x S_{\text{Tot}}}, \quad (3)$$

where  $Q^2$  is the negative four-momentum squared of the virtual photon and  $x$  is the Bjorken scaling variable. We also define  $W^2$ , the mass squared of the total hadronic system ( $X + \text{outgoing proton}$ ), by

$$W^2 = (P + q)^2. \quad (4)$$

Additionally, for diffractive scattering we define:

---

<sup>1</sup>920 GeV protons since August 1998.

$$t_P = (P - P')^2, \quad x_P = \frac{Q^2 + M_X^2}{Q^2 + W^2}, \quad \text{and} \quad \beta = \frac{Q^2}{Q^2 + M_X^2}, \quad (5)$$

where  $t_P$  is the momentum transfer at the proton vertex and is constrained by experimental cuts to be small ( $|t_P| \lesssim 1 \text{ GeV}^2$ ),  $x_P$  is the fraction of longitudinal momentum of the proton carried by the pomeron, and  $x = \beta x_P$ . The mass squared of the diffractive system  $X$  is  $M_X^2$ , and the proton mass is neglected.

The *pseudo-rapidity*,  $\eta$ , of an outgoing particle is defined in the laboratory frame in terms of its polar angle with respect to the proton direction by

$$\eta = -\ln \tan \left( \frac{\theta_{\text{lab}}}{2} \right). \quad (6)$$

### 2.1.2 Exchanged Quark Virtuality, Thrust and Transverse Momentum

For the leading-order (to order  $\alpha_s$ ) diffractive process shown in Fig. 1 we introduce a further invariant, the four-momentum squared of the struck quark,  $k^2$ . In the  $\gamma^* - \mathbb{P}$  CMS the virtuality of this quark can be expressed in terms of other invariants and the polar angle with respect to the  $\gamma^* - \mathbb{P}$  axis, by

$$k^2 = -\frac{Q^2 + M_X^2}{2}(1 - \cos \theta_{\text{cms}}). \quad (7)$$

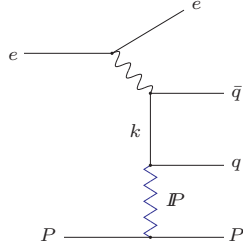


Figure 1: *Diffractive DIS via pomeron exchange.*

A similar expression can be formed for interactions where more than two diffractive final-state partons are produced.

There are two further quantities of interest here. The first is *thrust*,  $T$ , which describes the principal axis of jet momentum and the spread of final-state particles. More formally, the thrust axis is defined to be parallel to the vector  $\vec{n}$  which maximises the weighted sum

$$T = \left( \frac{1}{\sum_{i=1}^N |\vec{p}_i|} \right) \cdot \max_{\vec{n}} \sum_{i=1}^N |\vec{p}_i \cdot \vec{n}|, \quad (8)$$

where the sum is taken over the whole diffractive final state and  $T$  is the thrust variable<sup>2</sup>. The thrust axis in diffractive dijet production is the axis defined by the back-to-back final-state quarks in the virtual photon–pomeron CMS and is approximated experimentally by the thrust axis described by the (hadronic) diffractive final state. For a dijet event  $T$  is equal to 1, while for a symmetric 3-jet event  $T = 2/3$  and a completely isotropic multi-jet event will have  $T = 1/2$ . In general,  $T$  can take any value between  $1/2$  and 1.

Another useful kinematic quantity is the thrust transverse momentum,  $p_{\perp}^2$ , defined in the virtual photon–pomeron CMS. For events with dijet final states,  $p_{\perp}$  is simply the component of momentum of one of the final state hadronic jets which is transverse to photon–proton axis (equivalently, to the photon–pomeron axis<sup>3</sup>). This is shown in Fig. 2. In the more general case of final states with two or more partons, the experimentally measured transverse momentum variable is the transverse momentum of the thrust axis with respect to the photon–proton direction.

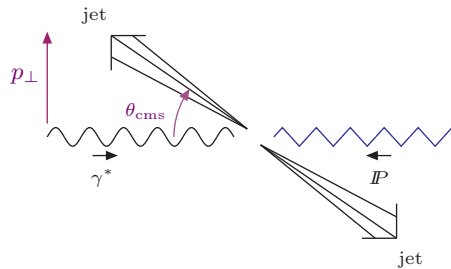


Figure 2: *Definition of transverse momentum variable  $p_{\perp}^2$  (in  $\gamma^* - P$  CMS).*

The transverse momentum variable defined above is different to that defined in [16] where phase space constraints due to pseudo-rapidity cuts [1, 9] are discussed in terms of a lower limit on the transverse momentum of the final-state parton which couples to the pomeron. The effect of pseudo-rapidity cuts on the 3-jet thrust transverse momentum distribution is more subtle as there exist 3-jet final-state configurations in which  $p_{\perp}^2_{\text{thrust}} = 0$ , for example, but for which the events will survive most pseudo-rapidity cuts. Events where there is a parton emitted far in the forward direction, however, are expected to be rejected by pseudo-rapidity cuts and hence there is likely to be a systematic reduction in the low- $p_{\perp}$  3-jet thrust transverse momentum spectrum. Constraints on thrust transverse momentum due to data selection cuts could, at best, be investigated through Monte Carlo studies of diffractive DIS.

### 3 Phase Space Analysis of Data Selection Cuts

We start this section with a summary of the data under investigation and then discuss the effects of the cuts used to select the diffractive DIS sample.

H1 measured the diffractive DIS cross section as a function of thrust transverse momentum,  $p_{\perp}^2$ , and final-state diffractive mass,  $M_X$ . They presented their results in the form [13]

<sup>2</sup>Some references use a slightly different definition of  $T$ . The normalisation of  $T$  we have adopted here is that used in [13].

<sup>3</sup>Here we assume that, for small  $t_P$ , the pomeron is emitted parallel to the proton direction.

$$\left. \frac{1}{\sigma} \frac{d^2\sigma}{dM_X^2 dp_\perp^2}(p_\perp^2) \right|_{\text{fixed } M_X}. \quad (9)$$

The diffractive cross section has been integrated over  $Q^2$  and  $x_{\mathbb{P}}$  in the range

$$\begin{aligned} Q^2 &: 10 \rightarrow 100 \text{ GeV}^2, \\ x_{\mathbb{P}} &: 10^{-4} \rightarrow 3.2 \times 10^{-2}, \end{aligned} \quad (10)$$

and the data was binned with average diffractive masses of

$$M_X = 7.01, 9.40, 12.82, 16.85, 21.20, 28.58 \text{ GeV}. \quad (11)$$

This corresponds to integrating over small values of  $\beta$ , for example: for  $M_X = 7.01 \text{ GeV}$ , over the range of  $Q^2$  in this analysis  $\beta$  ranges from 0.17 to 0.67; whereas for  $M_X = 28.58 \text{ GeV}$ ,  $\beta$  ranges from 0.01 to 0.11. Here “small” is to be interpreted as meaning values of  $\beta$  for which one might expect 3-jet processes to provide a significant contribution to the diffractive final state (specifically,  $\beta \lesssim 0.3$  [8]).

The H1 transverse momentum distribution data [13] has a  $1/p_\perp^2$  fall-off at low transverse momenta, steepening to a  $1/p_\perp^4$  fall-off at higher transverse momenta. This change in slope occurs between about  $1\text{--}10 \text{ GeV}^2$  for the values of  $M_X$  in this study. The  $1/p_\perp^4$  tail in the data is not a phase space effect, as this tail is present for all values of  $M_X$  a long way away from the phase space limit of  $p_{\perp\text{max}}^2 = M_X^2/4$ . For  $M_X = 28.58 \text{ GeV}$ , for example, the data changes slope at about  $p_\perp^2 = 10 \text{ GeV}^2$ .

In an analysis of this data one must take account of the effects of experimental cuts on the space of  $Q^2$  and  $x_{\mathbb{P}}$  which was integrated over. There are two cuts which restrict the accessible range of  $Q^2$  and  $x_{\mathbb{P}}$  for a given final-state transverse momentum and diffractive mass:

1. *Cut on  $y$ :  $y < 0.5$ .*

This cut is imposed to restrict the photo-production background, as well as removing events where the diffractive system is strongly boosted in the backward direction [13]. Using the relation (3) between  $y$  and the other kinematic variables we get the restriction on  $x_{\mathbb{P}}$ ,

$$x_{\mathbb{P}} > \frac{2(Q^2 + M_X^2)}{S_{\text{Tot}}}, \quad (12)$$

which corresponds to a lower limit on the integral over  $x_{\mathbb{P}}$  as a function of  $Q^2$  at fixed  $M_X$ .

2. *Pseudo-rapidity cut: require pseudo-rapidity gap greater than  $\eta_{\text{max}} = 3.2$ .*

It was shown in [9, 16] that imposing a pseudo-rapidity cut removes part of the low- $p_\perp$  dijet contribution to diffractive DIS. For a given range of kinematic variables  $Q^2$ ,  $M_X^2$  and  $x_{\mathbb{P}}$ , a pseudo-rapidity cut corresponds to imposing a lower transverse momentum cut-off,  $p_{\perp\text{min}}^2$ , on accepted events. Therefore, when calculating the cross section at a given  $p_\perp^2$ , say  $p_{\perp\text{fixed}}^2$ , one should only integrate over the region of  $Q^2$  and  $x_{\mathbb{P}}$  for which  $p_{\perp\text{min}}^2 < p_{\perp\text{fixed}}^2$ . The region of phase space for which  $p_{\perp\text{min}}^2 > p_{\perp\text{fixed}}^2$  will have been removed by the pseudo-rapidity cut.

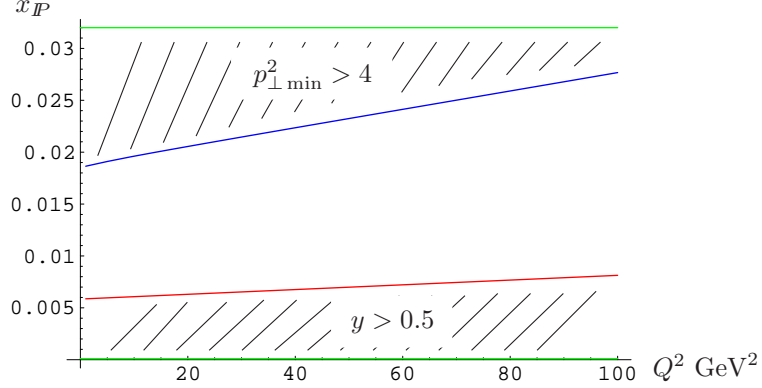


Figure 3: Phase space plot for  $p_{\perp \min}^2 = 4$ ,  $\eta_{\max} = 3.2$  (hadron-level cut), and  $M_X = 16$ . The horizontal lines show upper and lower limits of  $x_P$  in data sample, while the upper slanted line shows the upper limit on  $x_P$  as a result of pseudo-rapidity cuts, and the slanted lower line shows the lower limit of  $x_P$  as a result of the  $y$  cut.

The above discussion of the effect of pseudo-rapidity cuts on available phase space is illustrated in Fig. 3. In this figure, the region in the  $Q^2 - x_P$  plane over which one would integrate to extract the cross section at  $p_{\perp}^2 = 4 \text{ GeV}^2$  is shown for a diffractive mass of  $M_X = 16 \text{ GeV}$  and a pseudo-rapidity cut of 3.2 (typical HERA values). The upper shaded area shows the region excluded by the pseudo-rapidity cut. In this region of  $Q^2$  and  $x_P$  dijet events with  $p_{\perp}^2 < 4 \text{ GeV}^2$  are removed by the pseudo-rapidity cut. The lower shaded area shows the region excluded by the cut on  $y$ . As a result, there is a restricted region of phase space populated by dijet events with thrust transverse momentum of  $4 \text{ GeV}^2$ .

For large diffractive masses and small  $p_{\perp}^2$ , the data selection cuts exclude the entire  $Q^2 - x_P$  plane, leading to a sharp low-momentum cut-off in  $p_{\perp}^2$  below which there are no values of the kinematic parameters  $Q^2$  and  $x_P$  in the H1 study for which dijet events can contribute to the diffractive cross section. The position of the cut-off depends on  $M_X$ , and moves to larger transverse momentum values for larger diffractive masses. In Fig. 4, the position of the low-momentum dijet cut-off is shown for three diffractive masses:  $M_X = 28.58 \text{ GeV}$ ,  $21.20 \text{ GeV}$ , and  $16.85 \text{ GeV}$ . For smaller diffractive masses the transverse momentum distribution of dijet events is not strongly restricted by the data selection cuts and, for  $M_X \lesssim 15 \text{ GeV}$ , there is no lower  $p_{\perp}$  cut-off from the data selection cuts.

This analysis of the effect of data selection cuts on the dijet contribution to diffractive DIS therefore demonstrates that an additional contribution is needed to describe the H1 thrust transverse momentum distribution data, particularly at low transverse momenta.

## 4 Analysis of Diffractive Dijet Production Models

In this section we present the fits of various dijet models to the H1 thrust transverse momentum distribution data, starting with a brief description of the diffractive dijet models under consid-

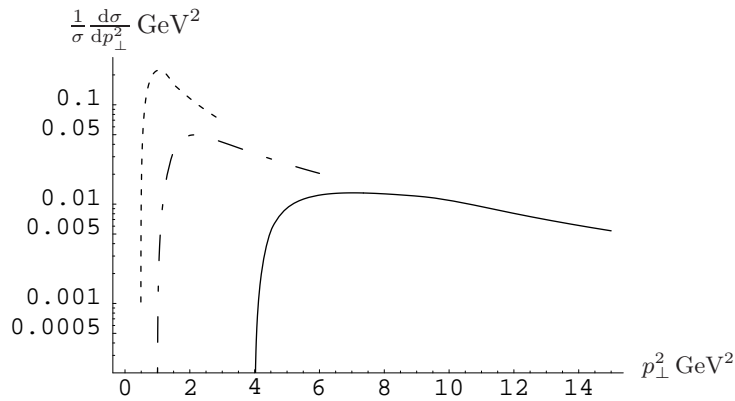


Figure 4: *Position of dijet transverse momentum cut-offs at different diffractive masses (two-gluon model). The solid line corresponds to a diffractive mass of 28.58 GeV, while the dot-dashed line is for 21.20 GeV, and the dotted line represents a diffractive mass of 16.85 GeV.*

eration. The contribution of higher-order diffractive processes, such as quark–antiquark–gluon diffractive final states, is discussed in the following section.

#### 4.1 Models of Diffractive Dijet Production

The first type of model we studied is the form factor approach of Donnachie and Landshoff [2,3] and Ellis and Ross [1,9] in which the diffractive interaction is assumed to proceed by the exchange of a  $C$ –even, vector-like pomeron. This approach allows for a direct coupling between the pomeron and off-shell partons. In order to maintain the experimentally-observed scaling of the diffractive structure function, a *form factor* is inserted to soften the virtual quark–pomeron vertex. In the original phenomenological model of Donnachie and Landshoff [2,3], applied to deep-inelastic scattering, one inserts a form factor at the virtual quark–pomeron vertex of

$$f(k^2) = \frac{\Lambda^2}{\Lambda^2 - k^2}. \quad (13)$$

Here  $k^2$  is the four-momentum squared of the exchanged quark coupling to the pomeron (the other quark at this vertex is near mass shell and hence its momentum may be neglected), and  $\Lambda^2$  is of the order of the hadronic scale ( $\Lambda^2 \sim 1 \text{ GeV}^2$ ). This serves to cut off contributions at large parton virtualities. In the modification suggested by Ellis and Ross [1], one chooses the form factor

$$f(k^2) = \sqrt{\frac{\Lambda^2}{\Lambda^2 - k^2}}. \quad (14)$$

This choice of form factor leads to a cross section with a logarithmic dependence on  $k^2$ , which therefore receives contributions from the entire  $k^2$  spectrum<sup>4</sup>. This model is motivated by

---

<sup>4</sup>Both form factor models reduce to the original Donnachie-Landshoff model of hadron-hadron scattering [17–20] for the exchange of a pomeron between two on-shell partons.



the observation that diffractive DIS is relatively insensitive to pseudo-rapidity [21–23], as well as the correlation between exchanged quark virtuality and pseudo-rapidity which was demonstrated in [9].

The other models we consider were described in detail in [9]. The first is a model in which the “pomeron” is described by the colour-singlet part of single-gluon exchange, that is, the exchange of one hard gluon with subsequent exchanges of soft gluons which “dress” the gluon colour enabling the formation of a pseudo-rapidity gap. We also consider a direct-coupling scalar pomeron model [4]. Finally, we consider the two-gluon Landshoff-Nachtmann model [5] following the analysis of Diehl [6]. In this approach the colour-singlet state is modeled by the exchange of two non-interacting gluons which are described by non-perturbative propagators and which are allowed to couple to the two quarks in all possible combinations.

It should be noted that the form factor models are not gauge-invariant [6, 7]. The sum of the diagrams which contribute to two-gluon exchange, as shown in Fig. 5, is an explicitly gauge-invariant quantity. Comparing the two approaches, the diagrams where the colour-singlet exchange is modeled by a hadron-like “pomeron” exclude the two diagrams in which the two gluons do not couple to the same quark line. At best, therefore, one might hope for the form factor models to be physically meaningful in a gauge where the contribution from these two diagrams is minimal. Diehl [7] has suggested a non-covariant gauge in which the D-L model mimics many of the features of the manifestly gauge-invariant Landshoff-Nachtmann two-gluon model. We find that studying the unintegrated transverse momentum distribution highlights the gauge non-invariance problem with the form factor approach, and we have chosen to calculate the form factor models in the non-covariant gauge in this analysis. We have also repeated the structure function analysis of [9] for the form factor models in this gauge (see Appendix).

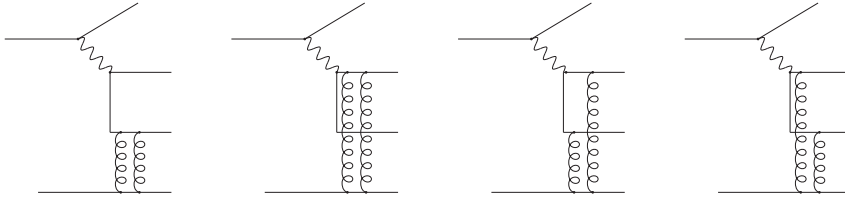


Figure 5: *Two-gluon exchange graphs used to model pomeron exchange.*

## 4.2 Transverse Momentum Distribution Fits with Dijet Models

The diffractive scattering cross section is calculated by integrating the cross section from the colour-singlet exchange models over the region of phase space in  $Q^2$  and  $x_{\mathbb{P}}$  accessed in the H1 analysis. The common feature of all the fits is that, as a result of the large pseudo-rapidity gap requirement and the cut on  $y$ , the dijet contribution is cut off sharply at low  $p_{\perp}^2$ . For example, for a diffractive mass of  $M_X = 28.58 \text{ GeV}$ , the phase space restrictions affect the dijet contribution below about  $10 \text{ GeV}^2$ , completely removing the contribution from events with  $p_{\perp}^2 \lesssim 4 \text{ GeV}^2$ . For  $M_X = 16.85 \text{ GeV}$ , the turn-over is much sharper and the spectrum cuts off between  $1\text{--}2 \text{ GeV}^2$ .

The curves in Figs. 6 and 7 represent the dijet model fits to the H1 data by fitting only the part of the curves after the phase space-induced turn-over. This shows how the models describe the large- $p_{\perp}^2$  behaviour of the cross section. In each graph the H1 data [13] is shown as solid points with error bars representing statistical and systematic errors added in quadrature.

The fits shown in Figs. 6(a) and 7(a) are of the Donnachie-Landshoff form factor model in the Feynman gauge (solid line) and in the non-covariant gauge (dashed line). In both cases we have assumed a pomeron intercept of 1.2 and a low-momentum cut-off in the form factor of  $\Lambda = 1.2 \text{ GeV}^2$ . These graphs show that the Donnachie-Landshoff model in the non-covariant gauge provides a good fit to the large- $p_{\perp}$  part of the transverse momentum spectrum, that is, it predicts a  $1/p_{\perp}^4$  fall-off for  $p_{\perp}^2 \gtrsim 10 \text{ GeV}^2$ . The Feynman gauge curve gives a poor fit, mainly due to a large- $p_{\perp}$  tail which is not present in the non-covariant gauge approach [7].

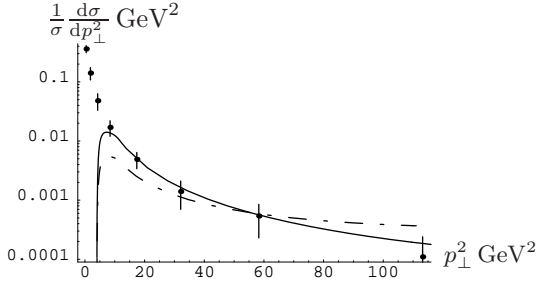
Figs. 6(b) and 7(b) show fits of the Ellis-Ross form factor model to the transverse momentum distribution data with  $\alpha_P(0) = 1.2$  and  $\Lambda = 1.2 \text{ GeV}^2$ . Again, a high- $p_{\perp}$  tail is evident in the cross section calculated in the Feynman gauge. The E-R model fails to describe the large transverse momentum behaviour of the data in either gauge, predicting a  $1/p_{\perp}^2$  fall-off at large transverse momenta. The scalar pomeron and single-gluon exchange models are shown in Figs. 6(c) and 7(c). These models also fail to describe the  $p_{\perp}^{-4}$  dependence of the data at large  $p_{\perp}^2$ , giving only a  $p_{\perp}^{-2}$  fall-off.

Finally, in Figs. 6(d) and 7(d) we study the two-gluon model of Diehl [6]. This model fits the data well above the phase space-induced low- $p_{\perp}$  cut-off. The fit here is similar to the fit obtained using the Donnachie-Landshoff form factor model.

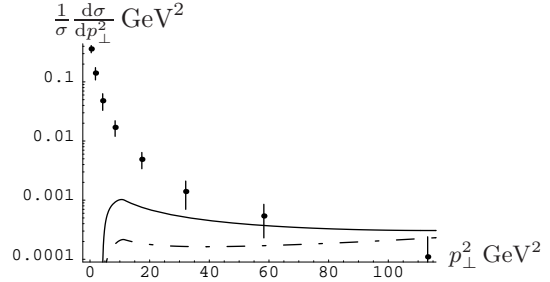
## 5 Comparison of Structure Function and Thrust Transverse Momentum Distribution Analyses

The results of fitting the colour-singlet exchange models to the thrust transverse momentum distribution data are surprising when compared with the results from the comparison of these models with the large pseudo-rapidity gap structure function data in [9]. The structure function data is obtained from the  $p_{\perp}$ -integrated cross section. The Ellis-Ross and single-gluon exchange models provided an acceptable fit to the large pseudo-rapidity gap structure function data, but did were unable to describe the shape of the thrust transverse momentum distribution data. By contrast, the Donnachie-Landshoff and two-gluon models fit the thrust transverse momentum distribution data well, but under-estimated the structure function data badly at low  $\beta$ . There are two possible ways to reconcile these results. The first possibility is that E-R and single-gluon exchange models may describe the data at large  $\beta$  (in the region where the operator product expansion is believed to be reliable in describing diffractive DIS), but that the leading-twist description fails at small  $\beta$ . The other possibility is that the D-L and two-gluon models are able to fit both sets of data with a substantial contribution from multi-jet diffractive final states. This latter possibility requires the multi-jet contribution to the low-momentum  $p_{\perp}^2$  data to be most significant at small- $\beta$  and to have a thrust transverse momentum distribution which is strongly peaked near zero.

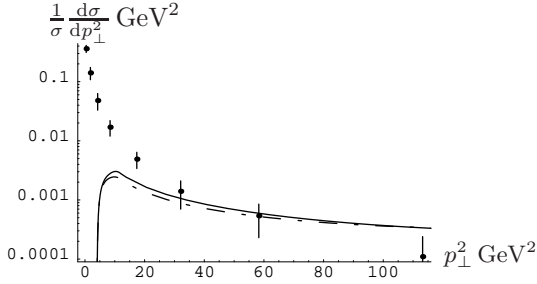
We discuss these possibilities in more detail in this section.



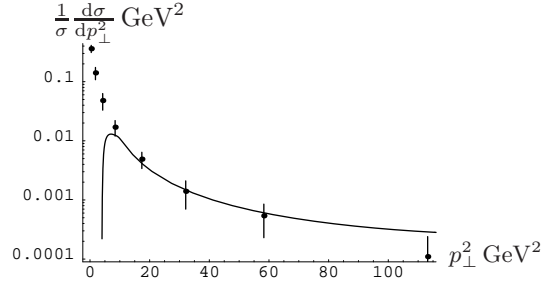
(a) *Donnachie-Landshoff form factor model in non-covariant gauge (solid line) and in Feynman gauge (dashed line). Here  $\Lambda = 0.2 \text{ GeV}^2$  and  $\alpha_P(0) = 1.08$ .*



(b) *Ellis-Ross form factor model in non-covariant gauge (solid line) and Feynman gauge (dashed line). Here  $\Lambda = 0.2 \text{ GeV}^2$  and  $\alpha_P(0) = 1.08$ .*

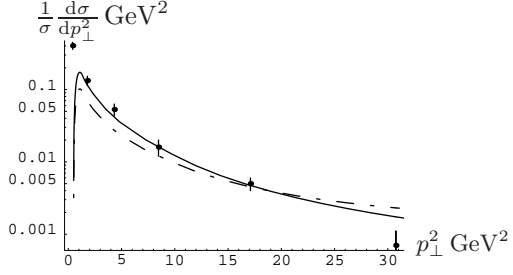


(c) *Single-gluon exchange model (solid line) and Scalar Pomeron exchange model (dashed line).*

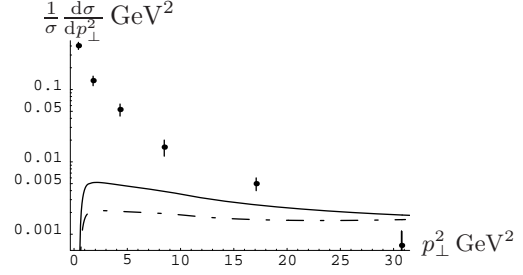


(d) *Two-gluon exchange model.*

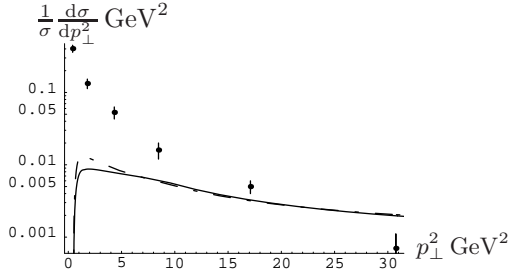
Figure 6: *Fits of colour-singlet exchange models to transverse momentum distribution data from [13]. The fit is made to points after the turn-over of the curves (see text for explanation). The curves correspond to the models, while the solid points are H1 data. The plots show the fits for diffractive masses in the region of  $M_X = 28.58 \text{ GeV}$ . The statistical and systematic errors have been added in quadrature.*



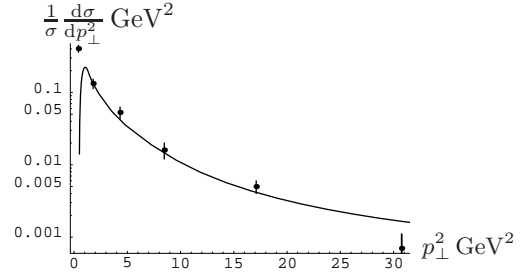
(a) *Donnachie-Landshoff form factor model in non-covariant gauge (solid line) and in Feynman gauge (dashed line). Here  $\Lambda = 0.2 \text{ GeV}^2$  and  $\alpha_P(0) = 1.08$ .*



(b) *Ellis-Ross form factor model in non-covariant gauge (solid line) and in Feynman gauge (dashed line). Here  $\Lambda = 0.2 \text{ GeV}^2$  and  $\alpha_P(0) = 1.08$ .*



(c) *Single-gluon exchange model (solid line) and Scalar Pomeron exchange model (dashed line).*



(d) *Two-gluon exchange model.*

Figure 7: *Fits of colour-singlet exchange models to transverse momentum distribution data from [13]. The fit is made to points after the turn-over of the curves. The curves correspond to the models, while the solid points are H1 data. The plots show the fits for diffractive masses in the region of  $M_X = 16.85 \text{ GeV}$ .*

## 5.1 $\beta$ -Dependent Structure Function Models

It is possible that the Ellis-Ross or leading-twist single-gluon exchange models describe a physical picture of the data for large  $\beta$ , but that some other (possibly higher-twist) component is required at low  $\beta$ . The E-R model provided a good fit ( $\chi^2/\text{dof} = 37/41$ ) to the large pseudo-rapidity gap structure function data studied in [9] and described the data well over a wide range of  $Q^2$ ,  $\beta$  and  $x_{\mathcal{P}}$ . Most of the large pseudo-rapidity gap structure function data is at low  $\beta$ , and the transverse momentum distribution data is almost all at low  $\beta$ , however, and there is not sufficient large- $\beta$  data available to test this possibility.

The present thrust transverse momentum distribution analysis demonstrates a need for a substantial extra non-dijet contribution to the cross section. Due to the low- $p_{\perp}$  dijet cut-off, some additional contribution is needed to explain the low transverse momentum data. The position of the cut-off shows also that the size of this extra contribution is  $\beta$ -dependent, and peaked at low  $\beta$ . If this low- $\beta$  contribution is included in the E-R model fits to large pseudo-rapidity gap structure function data it will cause the E-R model to overshoot the structure function data at low  $\beta$ . The need for a substantial low- $p_{\perp}$ , low- $\beta$  contribution to explain the thrust transverse momentum distribution data therefore presents a major challenge to E-R and leading-twist models.

## 5.2 Two-Gluon Dijet Contribution Plus 3-Jet Contribution

The  $M_X$ -dependent position of the dijet low transverse momentum cut-off is such that at large diffractive masses the region where dijet events cannot contribute to the diffractive scattering cross section is larger than for smaller diffractive masses. This dominance at small  $\beta$  is what is expected from quark-antiquark-gluon diffractive final states [8, 14, 15]. It seems reasonable therefore, given also the very small values of  $\beta$  in the H1 thrust study, to conclude that the extra contribution required to explain the thrust transverse momentum distribution spectrum is probably provided by 3-jet diffractive final-state events. This conclusion is consistent with [8], where it was estimated that the 3-jet contribution dominates the diffractive structure function for  $\beta \lesssim 0.2$ , and provides a significant contribution to  $F_2^{D(3)}$  for  $\beta \lesssim 0.4$ . This hypothesis is also consistent with the H1 findings that the average thrust of diffractive DIS events is less than 0.9 [13].

If the 3-jet contribution is indeed dominant at small  $\beta$  (large  $M_X$ ), one would expect to see the pattern of diffractive structure function results found in [9] for the D-L and two-gluon models. In this case the dijet contribution is expected to under-estimate the diffractive structure function at small  $\beta$ .

Here we discuss the low- $\beta$  component needed to give a good fit to the thrust transverse momentum distribution data. We assume in this discussion that the additional contribution at low- $\beta$  originates from quark-antiquark-gluon diffractive final states. Considering the results shown in Figs. 6 and 7, and the analysis in [9], one can immediately make two hypotheses about the distribution of “3-jet” processes in the diffractive sample:

- *3-jet events dominate the large pseudo-rapidity gap sample at low  $\beta$ :*

The requirement of a large pseudo-rapidity gap between the proton direction and the diffractive final state removes the low- $p_{\perp}^2$  dijet events from the sample [9, 16], hence higher-multiplicity

final states are required to explain the low transverse momentum part of the spectrum. Furthermore, comparing Figs. 6 and 7, we see also that the cut-off in the dijet contribution from the phase space restrictions is shifted to smaller  $p_{\perp}^2$  for smaller values of  $M_X$ . This is to be expected as smaller  $M_X$  corresponds to large values of  $\beta$ , for which there is a weaker restriction on the dijet phase space [9, 16]. Also the ratio of multi-jet events to dijet events is expected to be smaller at large  $\beta$  [8].

- *The thrust transverse momentum distribution of 3-jet events is strongly peaked about 0:*

This conclusion is partly based on the success of the two-gluon dijet model in fitting the  $p_{\perp}^{-4}$  behaviour of the cross section at large transverse momenta, and also on the inability of all the dijet models to describe the low- $p_{\perp}^2$  part of the spectrum due to data selection cuts. If the 3-jet events were to describe the part of the transverse momentum spectrum which is not described by dijet events, one would also require them to have thrust transverse momentum strongly peaked about  $p_{\perp}^2 = 0$ , in order to not effect the spectrum at larger transverse momenta.

A strongly peaked *thrust* transverse momentum distribution might be expected from a two-gluon “partonic” model of the pomeron. In such a model, the leading-order process is one where the photon interacts with one of the gluons in the pomeron, producing a diffractive quark–antiquark pair. The third final-state particle is the other constituent gluon in the pomeron, the pomeron remnant, which would be traveling in approximately the same direction as the initial proton. Therefore, especially if there is a reasonably isotropic distribution of momentum between the two constituent gluons in the pomeron, one would expect the thrust axis of the final state to be rather closely aligned with the proton–photon axis. This hypothesis does, however, require a  $\beta$ -dependent non-perturbative spreading of the transverse momentum distribution of the remnant gluon of up to  $p_{\perp}^2 = 6 \text{ GeV}^2$ . The intrinsic transverse momentum of the pomeron has been discussed recently in [24]. It is also possible that the peaked thrust transverse momentum distribution might be due to the non-zero momentum transfer at the proton vertex [25]. It is not possible to explore this latter possibility further at present as there is insufficient data describing the  $t_P$ -dependence of diffractive DIS.

### 5.2.1 Parameterization of the Extra Thrust Contribution

We fit the thrust transverse momentum distribution data with a combination of the two-gluon model and a parameterization for the “3-jet” contribution to diffractive DIS in which the invariant amplitude of the thrust transverse momentum distribution is described by the Gaussian<sup>5</sup>:

$$f(Q^2, \beta) = \frac{1}{Q^2 \beta} e^{-\frac{p_{\perp}^2}{\beta^2 p_{\perp, \text{max}}^2}}. \quad (15)$$

This provides a  $\beta$ -dependent distribution which falls sharply with increasing  $p_{\perp}^2$ . Since the H1 data contains no information about the absolute normalisation, in these fits the overall normalisation of each contribution is a free parameter, giving two adjustable parameters when combining the two contributions. The most unsatisfactory feature of the “3-jet” interpretation of

---

<sup>5</sup>Note that since the definition of the transverse momentum variable in this analysis is different to that used in the diffractive structure function study in [9], the parameterization used to fit the thrust transverse momentum distributions here cannot be directly applied to the structure function analysis.

this extra contribution is the need for an exponential  $\beta$ -dependent cut-off in the thrust transverse momentum distribution.

The combination fit is shown in Fig.8. This fit describes the transverse momentum distribution data well in the range of diffractive masses studied by H1, only underestimating the data slightly at  $M_X = 16.85 \text{ GeV}$ . This confirms that the data may be described by the combination of a dijet model with a quadratic fall-off with transverse momentum and a “multi-jet” parameterization with an exponentially decaying thrust transverse momentum distribution.

A more complete test of this hypothesis would be to study data for which the overall normalisation of the cross section at each diffractive mass is measured, as this would enable allow the relative contributions of 2- and 3-jet final states to the diffractive cross section to be measured.

## 6 Discussion and Conclusions

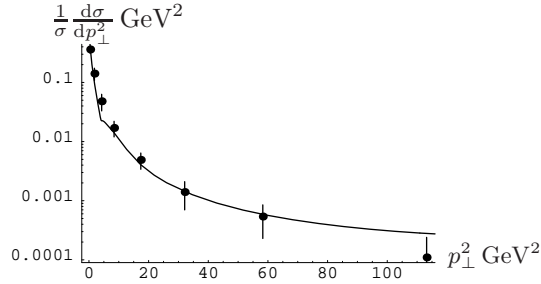
We have studied the transverse momentum distribution of diffractive DIS and compared the dijet component of several diffractive DIS models with recent H1 data [13].

The general trend in the data is towards a  $1/p_\perp^2$  fall-off at low transverse momenta, steepening to  $1/p_\perp^4$  at about  $4\text{--}10 \text{ GeV}^2$ . The position of the change in slope depends on the diffractive mass, with the change in slope occurring at larger values of the transverse momentum variable for larger  $M_X$ .

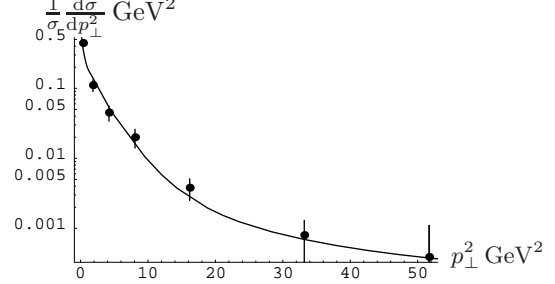
The data selection cuts, particularly the pseudo-rapidity cut imposed by H1 to select diffractive events, lead to a restriction on the available phase space for a wide of the parameter space covered by HERA. The main result is that, for most diffractive masses and for the range of  $Q^2$  and  $x_P$  in this analysis, data selection cuts are expected to remove all dijet events with small transverse momenta. As a result, one requires a further contribution, for example quark–antiquark–gluon final states, to explain the small- $p_\perp^2$  region of the H1 transverse momentum distribution data. The region in  $p_\perp$  where the data changes slope corresponds rather closely to the region where phase space effects due to data selection cuts remove the low- $p_\perp$  dijet contribution.

We compared four classes of colour-singlet exchange models with the H1 data: two form factor vector pomeron models, a leading-twist single-gluon exchange model, a scalar pomeron model, and a two-gluon exchange model. The cross section from the form factor models was calculated in both the Feynman gauge and in a non-covariant gauge. The difference between the two gauge choices was particularly evident in the large- $p_\perp^2$  tail which one obtains using the Feynman gauge, which is not seen in any other approach, and which fails to describe the present data. The Donnachie-Landshoff form factor model (in non-covariant gauge) provided a good fit to the large transverse momentum part of the spectrum for all values of diffractive mass beyond the point where the slope changed to a  $1/p_\perp^4$  fall. The Ellis-Ross form factor model, as well as the single-gluon and scalar pomeron models, predicts a  $1/p_\perp^2$  fall at large transverse momenta which is not consistent with the H1 data. The two-gluon model fit the large- $p_\perp$  part of the transverse momentum distribution spectrum well.

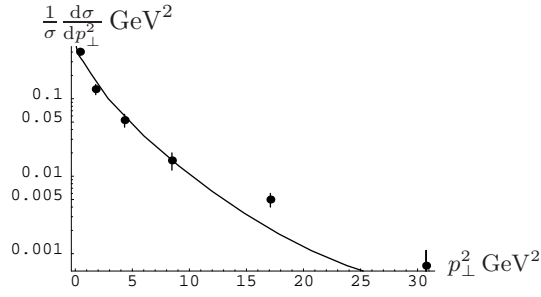
Since the region where dijet events cannot contribute to the diffractive cross section is much larger for larger diffractive masses (i.e. smaller  $\beta$ ), it was concluded that the extra contribution required to describe the H1 transverse momentum distribution data was probably from 3-jet diffractive final states. It was found that a combination of the two-gluon dijet model and a simple parameterization for the extra contribution using  $\beta$ -dependent Gaussian gave a good fit



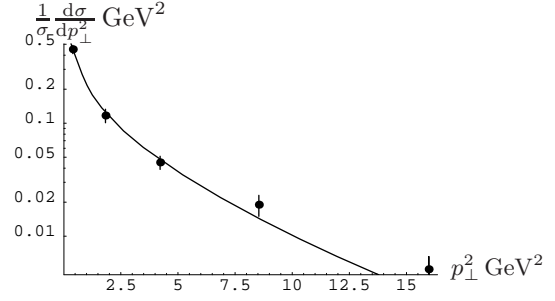
(a)  $M_X = 28.58$  GeV



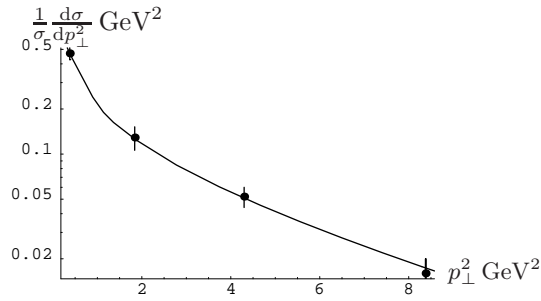
(b)  $M_X = 21.20$  GeV



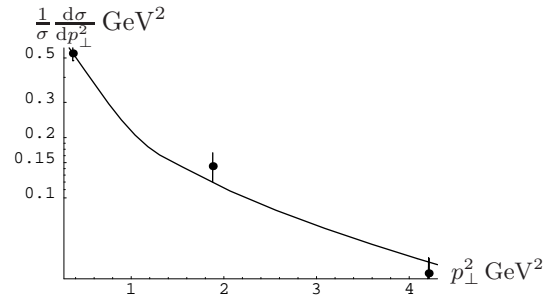
(c)  $M_X = 16.85$  GeV



(d)  $M_X = 12.82$  GeV



(e)  $M_X = 9.40$  GeV



(f)  $M_X = 7.01$  GeV

Figure 8: Comparison of the combination of a two-gluon dijet model and a 3-jet parameterization with thrust transverse momentum distribution data from [13] at different diffractive masses.



to the entire thrust transverse momentum distribution spectrum.

The 3-jet interpretation of this extra contribution is consistent with the earlier structure function analysis of large pseudo-rapidity gap diffractive DIS [9]. In this interpretation a large 3-jet diffractive contribution is required at small  $\beta$  in addition to the dijet contribution from the Donnachie-Landshoff or two-gluon models. In addition, however, the present analysis also requires the 3-jet diffractive events to have thrust transverse momentum strongly peaked about zero. This analysis also suggests that the apparent success of the Ellis-Ross, single-gluon and scalar pomeron models in describing the diffractive structure function may be due to these models over-estimating the large- $p_{\perp}^2$  dijet contribution.

An alternative possibility is that the E-R or leading-twist single-gluon models may provide a reasonable fit to the diffractive DIS cross section at moderate to large values of  $\beta$ . Present pseudo-rapidity gap thrust transverse momentum distribution and structure function data in which the requirement of a large pseudo-rapidity gap places strong restrictions on the available phase space corresponds mostly to small  $\beta$  and at present there is insufficient data, particularly at large- $\beta$ , to either prove or disprove these hypotheses.

This analysis demonstrates the worth of studying the transverse momentum dependence in distinguishing between models. Clearly it is of importance to obtain an improved data set in the diffractive scattering regime. In particular, it would be helpful if smaller  $x_{\mathcal{P}}$  data were available as the present jet production data has relatively large  $x_{\mathcal{P}}$  where the purely diffractive interpretation may be invalid.

Further investigation is required to test the hypotheses presented in this paper. On the theory side, there is a need for a full 3-jet diffractive DIS calculation or at least, as far as testing this analysis is concerned, for a proper Monte Carlo treatment of thrust transverse momentum distribution of 3-jet diffractive events with proper account taken of experimental data selection cuts. Better statistics and finer binning in the thrust transverse momentum variable would allow one to explore the interface between diffractive dijet production and the low- $p_{\perp}^2$  contribution. In a similar vein, analysing data corresponding to larger values of  $\beta$ , where phase space effects due to pseudo-rapidity cuts are less significant and dijet events are expected to dominate over higher-multiplicity diffractive final states, one would expect to see the quartic  $p_{\perp}$ -dependence in the present H1 data extend to smaller values of the  $p_{\perp}$ . On the other hand, restricting to smaller values of  $\beta$ , one would be able to push the position of the change to a quartic fall-off to larger values of  $p_{\perp}^2$ .

A more interesting experiment would be to keep the same range of kinematic parameters in  $Q^2$ ,  $\beta$  and  $x_{\mathcal{P}}$  and impose a strongly pseudo-rapidity cut. This would push the position of the low-momentum dijet cut-off to larger values of  $p_{\perp}^2$ . The only effect on the sharply-peaked low thrust- $p_{\perp}$  contribution would be a decrease in the overall normalisation. With fine enough binning in  $p_{\perp}$  this should therefore lead to the production of a “dip” in the cross section in the  $p_{\perp}^2$  region between where the exponential low- $p_{\perp}$  contribution cuts off and where the  $1/p_{\perp}^4$  dijet contribution starts.

Information about the overall normalisation of the cross section would enable the relative contributions of dijet and 3-jet events to diffractive DIS to be measured.

## Acknowledgments

Thanks to my collaborators, Graham Ross and John Ellis, and to Markus Diehl for helpful discussions. Thanks also to Ian Plummer for reading the manuscript and for very helpful comments. I am also very grateful for financial support from the NZFUW through an NZFUW Post Graduate Fellowship and a Sadie Balkind Scholarship.

## Appendix. Structure Function Analysis of Form Factor Models in Non-Covariant Gauge

This paper extends the form factor analysis of [9] to the non-covariant gauge choice described in [7]. It is interesting to see whether the form factor models describe the large pseudo-rapidity gap structure function data in this gauge. We have also repeated the structure function analysis for the form factor models with a low-momentum cut-off of  $\Lambda = 1.2 \text{ GeV}^2$  in the form factor, as suggested by fits to vector meson production data by Donnachie and Landshoff [2], rather than the smaller value of  $\Lambda = 0.2 \text{ GeV}^2$  used in the original pseudo-rapidity gap structure function analysis [9]. We compared the Donnachie-Landshoff and Ellis-Ross form factor models with the large virtuality constraint data from [26]. Fitting to the 42 points considered in [9], we obtained the  $\chi^2$  parameters shown in Table 1.

	$\chi^2/\text{dof}$	
	$\alpha_P(0) = 1.08$	$\alpha_P(0) = 1.2$
E-R: $f(k^2) = \sqrt{\frac{\Lambda^2}{\Lambda^2 - k^2}}$	39/41 (37/41)	57/41 (54/41)
D-L: $f(k^2) = \frac{\Lambda^2}{\Lambda^2 - k^2}$	81/41 (102/41)	79/41 (97/41)
E-R: (non-covariant gauge)	41/41 (41/41)	56/41 (55/41)
D-L: (non-covariant gauge)	69/41 (86/41)	68/41 (82/41)

Table 1: *Result of the fit of form factor models to large pseudo-rapidity gap diffractive structure function data from [26]. The fits assume a cut-off in the form factors of  $\Lambda^2 = 1.2 \text{ GeV}^2$ . Results of fits with a form factor cut-off of  $\Lambda^2 = 0.2 \text{ GeV}^2$  in the form factors, as was used in the original analysis in [9] are shown in brackets.*

We can see from Table 1 that changing the low-momentum form factor cut-off,  $\Lambda$ , and calculating the cross section in the non-covariant gauge make no real difference in the fits obtained in the Ellis-Ross model. The most significant effect on the Donnachie-Landshoff fits is from using the larger form factor cut-off. The D-L model, calculated in the non-covariant gauge with a form factor cut-off of  $\Lambda^2 = 1.2 \text{ GeV}^2$ , gives a moderately successful fit to the diffractive structure function data. The principal reason that the results for form factor cut-offs  $\Lambda^2 = 0.2 \text{ GeV}^2$  or  $\Lambda^2 = 1.2 \text{ GeV}^2$  are similar is that much of the data we are studying corresponds to an exchanged

quark virtuality of  $k^2 \gtrsim$  a few  $\text{GeV}^2$  in the form factors, hence the low-momentum cut-off in the form factor has little effect. The difference in the cross sections between using the Feynman gauge or the non-covariant gauge is visible when the unintegrated transverse momentum distributions are studied, as can be seen in the graphs in Sect. 4.

## References

- [1] J. Ellis and G. G. Ross, Phys. Lett. **B384**, 293 (1996).
- [2] A. Donnachie and P. V. Landshoff, Phys. Lett. **185B**, 403 (1987).
- [3] A. Donnachie and P. V. Landshoff, Phys. Lett. **191B**, 309 (1987).
- [4] J. Vermaseren, F. Barreiro, L. Labarga, and F. J. Yndurain, Phys. Lett. **B418**, 363 (1998).
- [5] P. V. Landshoff and O. Nachtmann, Z. Phys. **C35**, 405 (1987).
- [6] M. Diehl, Z. Phys. **C66**, 181 (1995).
- [7] M. Diehl, Eur. Phys. J. **C6**, 503 (1999).
- [8] J. Bartels, J. Ellis, H. Kowalski, and M. Wusthoff, Eur. Phys. J. **C7**, 443 (1999).
- [9] J. Ellis, G. G. Ross, and J. Williams, Eur. Phys. J. **C10**, 443 (1999).
- [10] A. Donnachie and P. V. Landshoff, Phys. Lett. **B285**, 172 (1992).
- [11] W. Buchmüller, M. F. McDermott, and A. Hebecker, Nucl. Phys. **B487**, 283 (1997).
- [12] W. Buchmüller, M. F. McDermott, and A. Hebecker, Phys. Lett. **B410**, 304 (1997).
- [13] H1, C. Adloff *et al.*, Eur. Phys. J. **C1**, 495 (1998).
- [14] M. Wusthoff, Phys. Rev. **D56**, 4311 (1997).
- [15] J. Bartels, H. Jung, and M. Wusthoff, hep-ph/9903265.
- [16] J. Williams, hep-ph/9905574.
- [17] A. Donnachie and P. V. Landshoff, Nucl. Phys. **B231**, 189 (1984).
- [18] A. Donnachie and P. V. Landshoff, Nucl. Phys. **B244**, 322 (1984).
- [19] A. Donnachie and P. V. Landshoff, Nucl. Phys. **B267**, 690 (1986).
- [20] A. Donnachie and P. V. Landshoff, Phys. Lett. **B296**, 227 (1992).
- [21] H1, T. Ahmed *et al.*, Nucl. Phys. **B429**, 477 (1994).
- [22] H1, T. Ahmed *et al.*, Nucl. Phys. **B435**, 3 (1995).
- [23] ZEUS, M. Derrick *et al.*, Phys. Lett. **B315**, 481 (1993).

- [24] N. N. Nikolaev, hep-ph/9905562.
- [25] ZEUS, J. Breitweg *et al.*, Eur. Phys. J. **C1**, 81 (1998).
- [26] J. P. Phillips, *The Deep-Inelastic Structure of Diffraction*, PhD thesis, University of Manchester, 1995, available from  
<http://www-h1.desy.de/h1/www/h1work/dif/publications.html>.